AGU ADVANCING EARTH AND SPACE SCIENCE

Geophysical Research Letters®

RESEARCH LETTER
10.1029/2021GL096170

Impact of Spreading Rate and Age-Offset on Oceanic Transform Fault Morphology

Yu Ren[1], Jacob Geersen[2], and Ingo Grevemeyer[1]

[1]GEOMAR Helmholtz Centre for Ocean Research Kiel, Kiel, Germany, [2]Institute of Geosciences, University of Kiel, Kiel, Germany

Key Points:

- We compiled multibeam bathymetric data of 94 oceanic transform faults (OTFs) to quantify their morphological characteristics
- Morphology of OTFs is dominated by age-offset rather than spreading rate
- Transform valleys get systematically deeper and wider with increasing age-offset, implying extensional tectonics at OTFs

Supporting Information:

Supporting Information may be found in the online version of this article.

Correspondence to:

Y. Ren,
yren@geomar.de

Citation:

Ren, Y., Geersen, J., & Grevemeyer, I. (2022). Impact of spreading rate and age-offset on oceanic transform fault morphology. *Geophysical Research Letters*, *49*, e2021GL096170. https://doi.org/10.1029/2021GL096170

Received 29 NOV 2021
Accepted 10 JAN 2022

Abstract Oceanic transform faults (OTFs) are an inherent part of seafloor spreading and plate tectonics, whereas the process controlling their morphology remains enigmatic. Here, we systematically quantify variations in transform morphology and their dependence on spreading rate and age-offset, based on a compilation of shipborne bathymetric data from 94 OTFs at ultraslow- to intermediate-spreading ridges. In general, the length, width and depth of OTFs scale systematically better with age-offset rather than spreading rate. This observation supports recent geodynamic models proposing that cross-transform extension scaling with age-offset, is a key process of transform dynamics. On the global scale, OTFs with larger age-offsets tend to have longer, wider, and deeper valleys. However, at small age-offsets (<5 Myr), scatters in the depth and width of OTFs increase, indicating that small age-offset OTFs with weak lithospheric strength are easily affected by secondary tectonic processes.

Plain Language Summary In the past 5 decades, studies on oceanic transform faults (OTFs) have revealed significant complexity in their morphology, which calls for detailed quantitative analysis to study the processes controlling the morphology of OTFs. Using the most complete and advanced compilation of bathymetric data from ultraslow- to intermediate-spreading ridges, we parameterized the morphological characteristics of OTFs and extracted length, width and depth for each transform fault from the compiled bathymetric data. Moreover, correlations between these morphological parameters and related tectonic factors (e.g., spreading rate, age-offset) were investigated in this study. We find that correlations between morphological features and spreading rate are rather weak. Comparison of correlations suggests that age-offset scales better with the morphological parameters, along with scatters mostly at small age-offsets, indicating small-age-offset OTFs are unstable due to their weak lithospheric strength. Our observation evidences extensional tectonics at OTFs.

1. Introduction

Oceanic transform faults (OTFs) are prominent linear features in the ocean-basins, offsetting mid-ocean ridges by tens to several hundreds of kilometers and hence juxtaposing oceanic lithosphere of contrasting age (Fox & Gallo, 1984; Wilson, 1965). They are usually located in remote oceanic regions where coverage from high-resolution shipborne bathymetric data is often rather poor. In the past decades, the quantity and quality of shipborne bathymetric surveys mapping the remote seafloor has, however, steadily increased (Gallo et al., 1986; Pockalny et al.,1988; Ryan et al., 2009). The new data revealed an enormous variability with respect to the morphology of global OTFs, calling for updated tectonic models on the origin of OTFs and their role in plate tectonics (Furlong et al., 2001; Gerya, 2012; Searle, 1986; Wolfson-Schwehr & Boettcher, 2019).

Unfortunately, even more than 5 decades after Wilson (1965) published his landmark paper on OTFs, we have a limited understanding of the processes controlling their morphological variability. Conceptually, they are simple conservative strike-slip faults and inherent to the spreading process (Sandwell, 1986; Sykes, 1967; Wilson, 1965). However, the strike-slip fault of a transform system often runs along a transform valley (Wolfson-Schwehr & Boettcher, 2019) which is several kilometers wide (e.g., Searle, 1986) and processes shaping these valleys are poorly understood. In addition, small changes in plate motion may result in either extension across OTFs, curving J-shaped abyssal hills at the ridge-transform intersections (Fornari et al., 1989; Tucholke & Schouten, 1988), widening the valley, the formation of transverse ridges (Pockalny et al., 1996), or causing compressive features within the transform valley (Harmon et al., 2018; Maia, 2019). However, recent observations suggest that the formation of transform valley might be inherently related to extensional tectonics at OTFs (Grevemeyer et al., 2021).

Geodynamic modeling suggests that the nonlinear viscoplastic rheology of oceanic lithosphere governs deformation below the rectilinear strike-slip plate boundaries, causing extension and thinning of the crust and hence wide and deep valleys (Grevemeyer et al., 2021).

Such geodynamic models require observational evidence to benchmark them (Ito, 2021). A previous statistical study has indicated that the length of OTFs is poorly correlated to spreading rate (Sandwell, 1986). More recent statistical compilations have shown that the width of OTFs may increase with spreading rate (Dauteuil et al., 2002) and age-offset (Luo et al., 2021) or that the depth of transform valleys scales with spreading rate and age-offset (Grevemeyer et al., 2021). However, it should be noted that observational studies of transform morphology and their dependence on related tectonic features generally suffer from poor data quality, coverage and/or lacked resolution (Text S1 in Supporting Information S1) and thus may bias our perception of ridge-transform dynamics (Luo et al., 2021).

The objective of this paper is to quantify variations in the morphology of global OTFs and to systematically study their dependence on related tectonic parameters, including spreading rate and age-offset. We collected and analyzed multibeam bathymetric data of 94 OTFs (Figure 1a) from ultraslow- to intermediate-spreading ridges. OTFs corresponding to higher spreading rates were excluded because their morphology and segmentation are often rather complex and thus may not allow a simple quantification (e.g., Dauteuil et al., 2002; Fox & Gallo, 1984). Our results provide new insights into the systematic variation of transform morphology and parameters governing key features like the width and depth of transform valleys.

2. Data and Methods

We compiled and merged shipborne multibeam bathymetric data from the Global Multi-Resolution Topography (GMRT) synthesis (Ryan et al., 2009) and the Japan Agency for Marine-Earth Science and Technology (JAMSTEC). Data from these databases were complemented with bathymetric information from several individual research cruises which were carried out in the region of the Bouvet triple junction (Ligi et al., 1999), along the Romanche (Ligi et al., 2002), St. Paul (Maia et al., 2016), and Chain (Harmon et al., 2018) transforms, as well as along the Central Indian Ridge (Okino et al., 2015). All the data were quality checked and regridded to a 100-m cell size for further processing and analyzing by using the ArcGIS Desktop software. Based on this compilation, we were able to generate maps of shipborne bathymetry for 94 OTFs, including 8 OTFs from the ultraslow-spreading Southwest Indian Ridge, 30 OTFs from the slow-spreading Central Indian Ridge and Mid-Atlantic Ridge, and 56 OTFs from the intermediate-spreading Southeast Indian Ridge, Chile Rise, Pacific Antarctic Ridge, Juan de Fuca Ridge, and Galapagos Ridge (Figure 1a).

We used the merged bathymetric datasets to study the systematics of OTFs, including length, width, depth, and their standard deviation. Figures 1b–1e illustrate characteristic structural elements of OTFs for the Chain transform (Figures 1b–1d) and the Chiloe transform (Figure 1e). At mid-ocean ridges, an active OTF is bounded by the two ridge-transform intersections (RTIs), where the tectonic stresses rotate over tens of degrees from ridge normal extension to strike-slip motion along the OTF (Figure 1b). Thus, the length of an OTF can be best defined by the distance between the two RTIs. Unfortunately, most OTFs and adjacent mid-ocean ridges lack high-resolution magnetic data to define seafloor ages along OTFs (Text S2, Figure S1, and Table S1 in Supporting Information S1). We therefore defined the age-offset as the transform fault length divided by the half-spreading rate derived from MORVEL (DeMets et al., 2010). While the length of an OTF can readily be derived, the rugged morphology of transform domains calls for a robust definition of key parameters like depth and width. At intermediate, slow and ultraslow spreading rates, the transform fault generally runs along a deep transform valley, which is usually flanked by the abyssal hills, transverse ridges, or oceanic core complexes developing at inside corner setting. From both bounding walls, the seafloor slopes steeply down into the transform valley. The slope map of the Chain transform (Figure 1c) highlights the transition from the steep slopes of the flanking valley walls to the flat seafloor of the valley. We used this characteristic feature to derive the outline or perimeter of the valley, including additional tectonic features such as submarine volcanos or flower structures (Figure 1b) in the deep valley. Thus, we calculated the slope gradient of the seafloor and manually defined a polygon (in red color, Figure 1b) at the toe of the steep slope of the valley walls where the seabed grades into a flat or gently sloping floor within the valley. Toward the RTIs, the polygon is truncated by two parallel lines perpendicular to the long axis of the transform fault, at a distance of 5–15 km from the RTIs to avoid morphological edge effects (DeMets

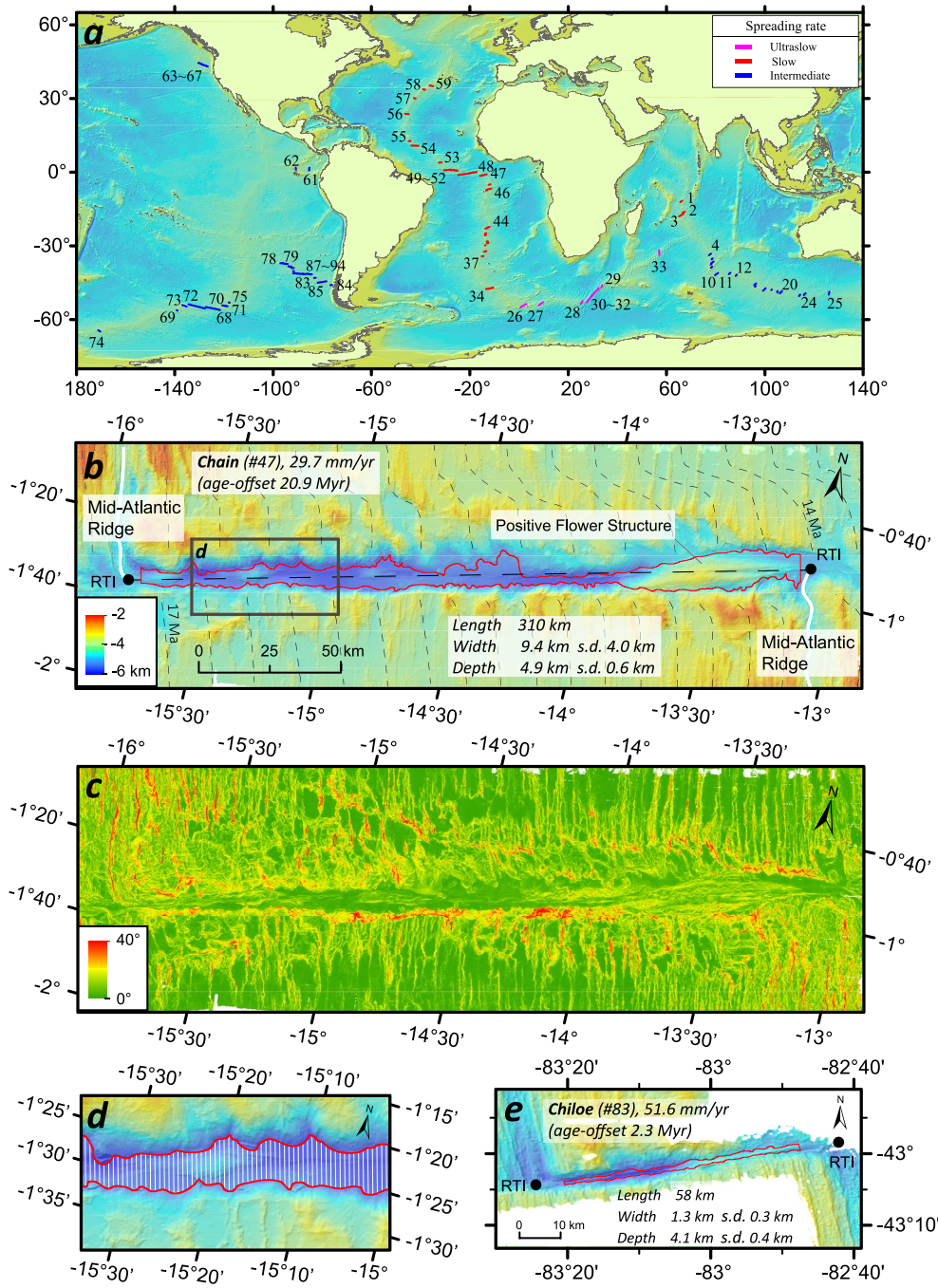

Figure 1. (a) Locations of the 94 oceanic transform faults (OTFs) investigated in this research. Numbering is as in column 1 of Table S2 in Supporting Information S1. (b) Bathymetry (from Harmon et al., 2018), (c) Slope map and (d) Zoomed bathymetric view of the Chain transform. Dashed lines on the opposite plates are age contours at 1 Ma interval from global age grid (Seton et al., 2020). Location of the Chain transform can be traced in panel (a) with its numbering (#47). Black box: the region shown in the zoomed view in (d). The white parallel lines at 1 km spacing which trend perpendicular to the long axis of the OTF (black dashed line in b) are used to derive the width of the transform. They are truncated on both sides by the outline of the transform valley (red lines). (e) Bathymetry (from GMRT synthesis, Ryan et al., 2009) of the Chiloe transform (#83). Color scale is the same as in panel (b). RTI, ridge-transform intersection; s.d., standard deviation.

et al., 2010; Grevemeyer et al., 2021). In the case of Chain transform fault, ridge axis at the RTI curves into the deep valley, causing J-shaped abyssal curvatures within a distance of ~5 km from the RTI. Thus, the polygon outlining valley wall scarps was truncated by two vertical lines of the transform axis at a distance of 5 km from

both RTIs (Figure 1b). To derive the width of the transform valley, we used parallel lines at 1 km spacing which trend perpendicular to the transform axis. The lines are truncated on both sides by the outline of the transform valley (red lines, Figure 1d). The width is then defined as the mean length of these truncated lines, from which the standard deviation is also measured. Using ArcGIS, data points from the bathymetry inside of the polygon were extracted and used to derive mean depth and its standard deviation. Besides, the area, perimeter and area/perimeter ratio of the outline of the transform valley were also measured in this study.

3. Results

A summary of the morphologic parameters for each OTF is presented in Table S2 in Supporting Information S1. Spreading rate across the 94 investigated OTFs varies from 14.1 to 83.1 mm/yr. The related age-offset ranges from 0.6 to 62.2 Myr. From the OTFs, 92 (97.9%) have an age-offset of less than 30 Myr and only two exceed 55 Myr (Andrew Bain W, 62.2 Myr; Romanche, 58.0 Myr). The length of OTFs varies from 21 to 847 km, with an average of ∼118 km. The longest one is the Romanche transform at the equatorial Mid-Atlantic ridge. From all transforms studied, 86 OTFs (91.5%) are shorter than 250 km. The width of the OTFs varies from 0.9 to 15.1 km, with an average of ∼3.7 km. The Vema transform, also at the equatorial Mid-Atlantic ridge, is the widest known OTF on Earth. From the investigated OTFs, 75 (79.8%) are narrower than 5 km. The mean water depth of the OTFs varies from 2.3 to 5.6 km, with an average of ∼3.8 km. Again, the Romanche transform has the deepest seafloor within the transform valley, up to ∼7,860 m.

An interesting feature is the large variability of morphologic parameters (especially the width) at slow spreading rates (Figures 2a–2c, Figures S2a–S2c and S3 in Supporting Information S1). Length, width, and depth ranges of OTFs at ultraslow-spreading Southwest Indian Ridge are 91–438 km, 4.3–10.5 km, 3.9–5.6 km, respectively. Table S3 in Supporting Information S1 documents the average morphologic variations subdivided into OTFs from ultraslow- (0–20 mm/yr), slow- (20–50 mm/yr) and intermediate- (50–90 mm/yr) spreading ridges. OTFs from ultraslow-spreading ridges share the largest mean values in age-offset (26.2 Myr), length (189.7 km), width (7.1 km) and depth (5.1 km), while the intermediate-slipping OTFs have the lowest mean values in transform parameters (3.2 Myr, 100.7 km long, 2.4 km wide, 3.5 km deep). To investigate their specific dependence on spreading rate and age-offset, we systematically plotted the length, width and depth of all OTFs against the spreading rate (Figures 2a–2c) and age-offset (Figures 2d–2f), and calculated the weighted linear fits with 95% confidence intervals.

We observed large scatters in Figures 2a–2c. Slopes of the linear fits are all negative. For length and width, this feature is superimposed by an inverse and hence positive trend (increase) for OTFs that share a similar age-offset (same color in the plot). This increase is most obvious for OTFs with age-offsets above 5 Myr whereas below 5 Myr a large scatter prohibits the identification of robust patterns (Figures 2a and 2b). With respect to the depth (Figure 2c), there seems to be an overall decrease in average water depth with increasing spreading rate, which is more obvious compared to the length and the width. However, a systematic increase in depth for OTFs with similar age-offsets, as observed for width and length, is not evident from the plot. Values of the coefficient of determination (R^2) are all small, indicating that correlations between morphologic parameters and spreading rate are rather weak.

The length, width, and depth patterns are different if plotted against the age-offset (Figures 2d–2f). Transform length increases with increasing age-offset on a global scale as well as almost linearly if considered for OTFs originating at the same spreading ridge. Both width and depth increase at OTFs with age-offsets above 5 Myr (Figures 2h and 2i). The improved R^2 value suggests that correlations between morphologic parameters and age-offset are reasonably stronger. Furthermore, width scales with age-offset better than depth, according to the R^2. The scatter discussed above for small-age-offset (<5 Myr) OTFs is, however, still visible (Figures 2e, 2f, and 3a–3c). The width of small-age-offset OTFs varies from 0.8 to 5.1 km, while the width of large-age-offset (>5 Myr) OTFs ranges from 1.7 to 15.1 km. The average water depth of small- and large-age-offset OTFs varies from 2.3 to 4.8 km and 2.6–5.6 km, respectively. Furthermore, large age-offset OTFs tend to slip at slow rates (Figure 3d, Figure S6 in Supporting Information S1), which agrees with the simplified calculation of age-offset by dividing transform length by half-spreading rate.

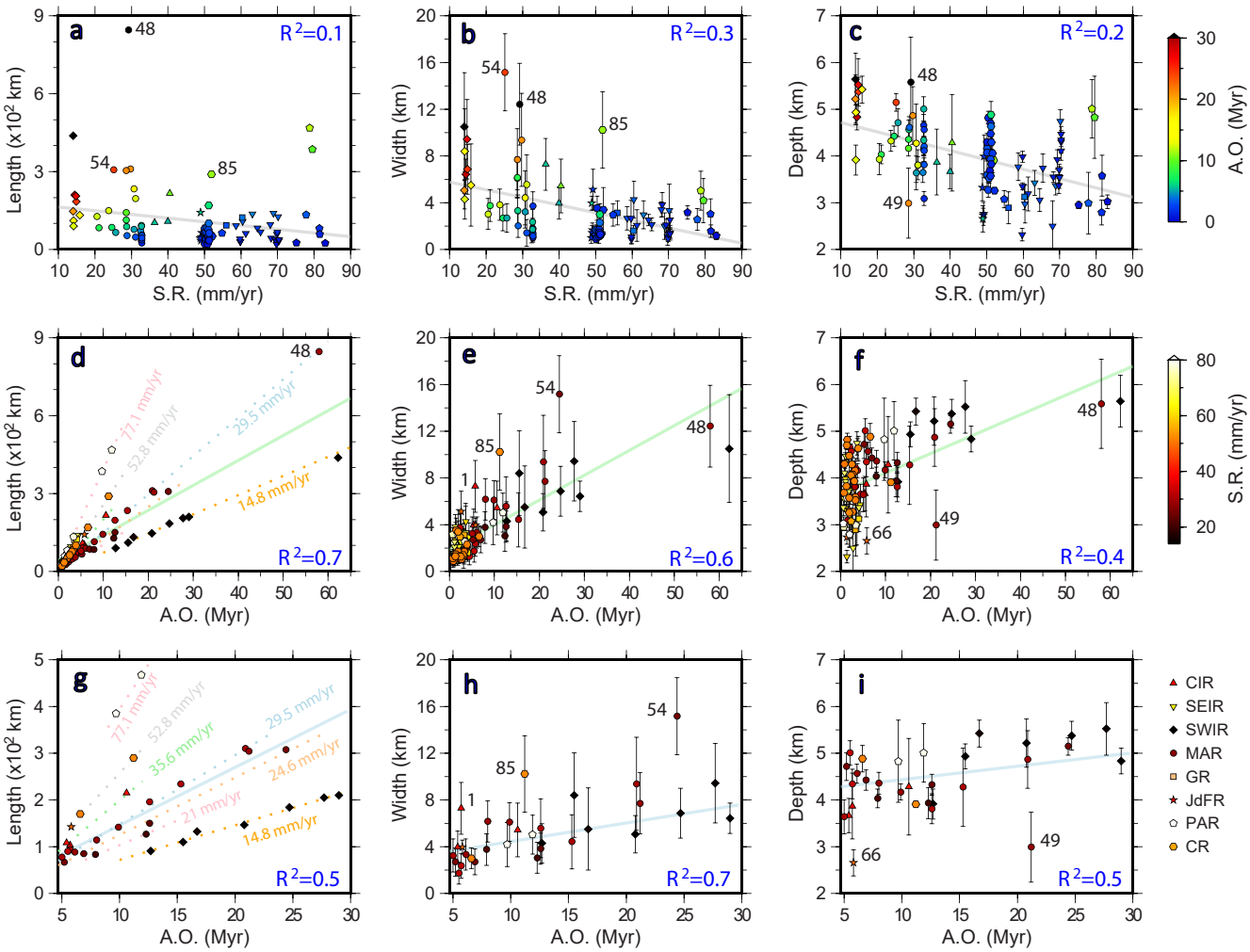

Figure 2. Morphological variability of global oceanic transform faults (OTFs). (a–f) Length, mean width, and mean water depth of OTF versus spreading rate and age-offset, respectively. (g–i) Zoomed views of (d–f). Thick lines show weighted linear fits. In figures (h–i) OTFs labeled (Table S5 in Supporting Information S1) which have undergone obvious secondary processes discussed were excluded during calculating their linear fits. A.O., age-offset; S.R., spreading rate. CR, Chile Rise; PAR, Pacific Antarctic Ridge; JdFR, Juan de Fuca Ridge; GR, Galapagos Ridge; MAR, Mid-Atlantic Ridge; SWIR, Southwest Indian Ridge; SEIR, Southeast Indian Ridge; CIR, Central Indian Ridge. 1, CIR 12S; 48, Romanche; 49, St Paul A; 54, Vema; 66, Blanco D; 85, Guafo.

4. Discussion

4.1. Comparison With Previous Statistics on the Morphology of OTFs

In an early study, Sandwell (1986) used bathymetry and satellite altimeter data to measure the length of global OTFs, and only found a weak correlation between transform length and spreading rate. The width of 24 OTFs was studied by Dauteuil et al. (2002) and they suggested that width correlates with spreading rate, despite a high variability resulting from secondary processes affecting the local lithospheric strength. Using a compilation of 41 well-mapped OTFs, Grevemeyer et al. (2021) revealed that the depth of transform valleys is generally much deeper at slow- and ultraslow-spreading rates than at intermediate- and fast-spreading rates. Such observations are also supported by a recent study (Luo et al., 2021), suggesting that the width and depth of OTFs decrease with increasing spreading rate. However, Luo et al. (2021) reported only 44 width estimates and their approach used the SRTM15+ bathymetry (Tozer et al., 2019) instead of using swath-mapping data and hence their estimates might be biased by including predicted seafloor bathymetry. Furthermore, they defined the width by the distance between the crests of the flanking walls of the OTF instead of using the width of the transform valley floor. Consequently, their estimates are two to three times wider than our estimates and values reported by Mishra and Gordon (2016) (Figure S5 in Supporting Information S1). Further, Luo et al. (2021) defined the width by a single

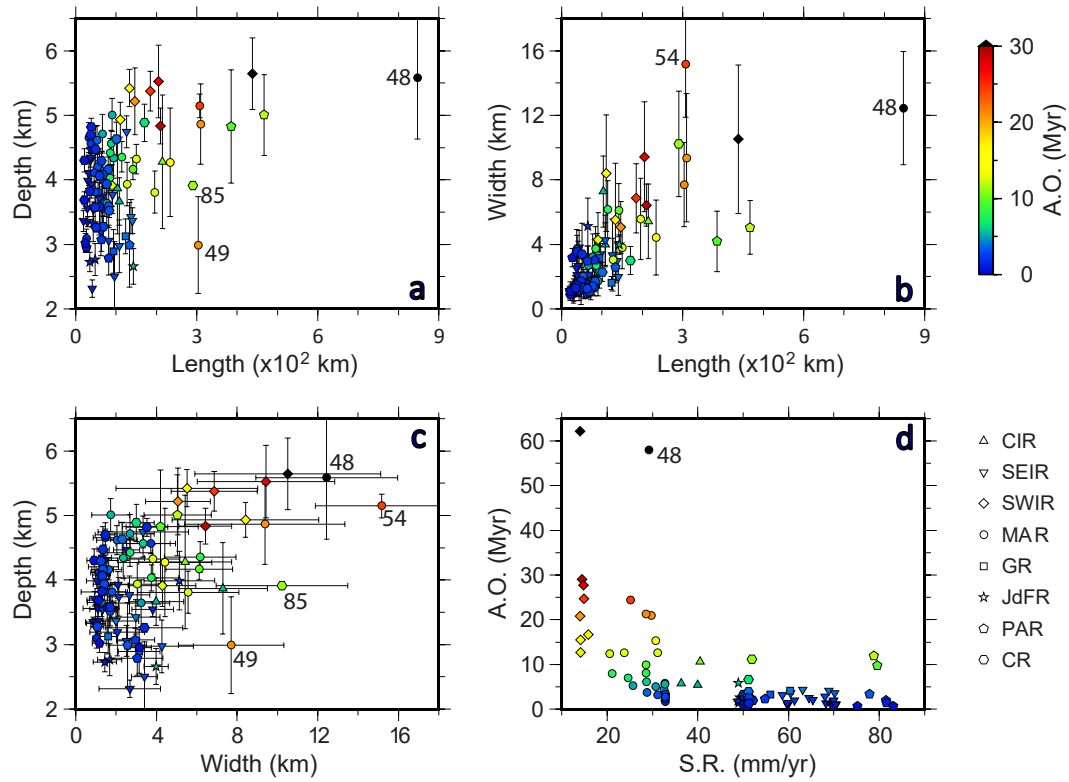

Figure 3. Correlations between morphologic parameters of global oceanic transform faults (OTFs). (a) Depth versus length. (b) Width versus length. (c) Depth versus width. (d) Age-offset versus spreading rate. Numbering is consistent in Figures 1a and 2.

measurement at the center of the OTF and Mishra and Gordon (2016) used the width of a best fitting rectangular instead of using a statistically robust approach (e.g., our polygon outlining the shape of transform valley). Similar simplifications not only governed width but also depth estimates of most previous approaches (Text S1 in Supporting Information S1). Therefore, statistically robust estimates from this study are needed to further explore transform tectonics.

4.2. Spreading Rate and Age-Offset Dependence of Transform Morphology

Our documented spreading rate dependence of transform morphology is consistent with the above-mentioned studies. Slow spreading rates correspond to large age-offsets as well as long, wide, and deep valleys. However, the low values of the coefficient of determination (R^2) for the length, width, and depth suggest that their correlations with spreading rate are reasonably weak, as they are superimposed by a high degree of scattering (Figures 2a–2c). It is worth noting that the scatters in our data also comply with previous studies (Dauteuil et al., 2002; Grevemeyer et al., 2021; Luo et al., 2021; Sandwell, 1986), indicating that other processes further affect transform morphology.

Correlations between age-offset and transform morphology are more robust. The age-offset is derived from transform length and spreading rate. It is therefore obvious, that an increase in age-offset corresponds to a linear increase in transform length, for a given spreading rate (Figure 2d). However, the high R^2 (0.7) for length could be biased by the cluster at small age-offsets, since the R^2 decreases at larger age-offsets (Figure 2g). For width and depth, R^2 values increase at age-offsets above 5 Myr (Figures 2h and 2i). OTFs with large age-offsets tend to slip at lower rates, corresponding to long, wide, and deep valleys. With respect to other statistical studies (Text S1 in Supporting Information S1), our data set shows a more consistent and clearer age-offset dependence of transform morphology (Figure S5 in Supporting Information S1). Using the most complete and advanced data set on transform morphology compiled so far, we confirm that morphological parameters correlate well with age-offset, indicating that the age-offset plays an important role in the ridge-transform dynamics. The fact that the spreading

rate and transform length are used for calculating the age-offset explains the long-wavelength dependence of transform morphologic parameters on spreading rate (Figures 2a–2c) or transform length (Figures 3a and 3b) despite the obvious large scatters.

4.3. Implications for the Transform Dynamics

Previous geophysical studies uncovered that thinning and stretching represent typical tectonic process within OTFs. For example, seismic refraction (Whitmarsh & Calvert, 1986) and gravity studies (Brink et al., 2002; Escartín & Cannat, 1999) revealed very thin crust along the transform valley. Moreover, normal faulting and stretching within OTFs was directly observed in several microseismicity studies (Cessaro & Hussong, 1986; Wilcock et al., 1990; Yu et al., 2021). Global analysis of the azimuths of OTFs suggested that transforms do not precisely parallel plate motion (Mishra & Gordon, 2016), thus their deformation could partly be accommodated by stretching along the OTFs.

Numerical simulations further revealed extensional tectonics within transforms. Within the ridge-transform system, the adjacent old and cold lithosphere lowers the temperature in the wedge of asthenosphere rising beneath the ridge axis (Collette, 1974; Fox & Gallo, 1984). The lateral cooling and heat conduction result in thermal stress across the transform, which in turn affects the structure of OTFs (Morgan & Forsyth, 1988; Turcotte, 1974). According to results from thermal models, Collette (1974) suggested that OTFs are contraction cracks relieving thermal stress, causing the shrinkage of opposite lithospheric plates. This might be responsible for the wide and deep valley within the ridge-transform system (Sandwell, 1986). Further, thermal (Furlong et al., 2001) and geodynamic flow models (Grevemeyer et al., 2021) proposed the existence of an oblique shear zone at depth, which infers an extensional component within the transform domain. The extensional tectonics at OTFs correspond to oblique faulting at shallow depth (Mishra & Gordon, 2016), mantle upwelling and/or crustal thinning along the transform, and hence widening and deepening of OTFs (Furlong et al., 2001; Grevemeyer et al., 2021). Further, geodynamic models predict that the cross-transform extension, a key process of transform dynamics, scales with the age-offset (Grevemeyer et al., 2021).

In this study, the robust correlation between transform morphology and age-offset, especially for large-age-offset OTFs, links the extension predicted by geodynamic simulations to the surface deformation pattern. The overall increase in the morphological parameters of global OTFs with increasing age-offset as well as the robust R^2 values support the hypothesized extensional tectonics at OTFs (Grevemeyer et al., 2021) in a statistical manner. The cross-transform extension, scaling with age-offset and predicted by thermal contraction, is an important process acting on oceanic transform plate boundaries. However, the large variability revealed in the cross plots (Figures 2e, 2f, and 3a–3c) supports that both width and depth of transform valleys are affected by secondary tectonic processes that may act independently.

4.4. Processes Affecting Transform Morphology

Another key observation with respect to transform morphology is the fact that width and depth show significantly more scatters for small-age-offset (<5 Myr) OTFs than for OTFs with age-offsets above 5 Myr (Figures 2e, 2f, and 3a–3c). One explanation for the scattering at small age-offsets is the time-delay until a tectonic process is reflected in surface morphology which can actually take hundred-thousand to millions of years (Gerya, 2010, 2013). Considering the extensional effect of OTFs, it may thus take a certain time until widening and deepening of the transform valley has reached a threshold that can be identified in seafloor morphology (Sandwell, 1986). Especially considering that the morphology of newly generated lithosphere that becomes subject to transform related processes, may differ between different spreading segments.

In addition, we also observed (Figure 3d and Figure S6 in Supporting Information S1) that the majority of small-age-offset OTFs slip at faster rates, while most transforms with large age-offsets correspond to slower spreading rates. Moreover, analogue and numerical models (Dauteuil et al., 2002; Furlong et al., 2001) have indicated that small-age-offset transforms tend to be hotter and more ductile to accommodate the higher spreading rate than OTFs with large age-offsets. Therefore, OTFs with small age-offsets are more likely altered by secondary tectonic processes, which can be caused by the stress field adjustment, or the regional variations in mantle temperature or composition. In the following, we evaluate secondary processes which may alter transform morphology.

Properties of OTFs might be affected by regional features, like hotspots, which may increase the melt supply and by this generate warmer thermal conditions at nearby transform faults. This may lead to anomalous thickening of the crust and thus shallower transform valleys (Dauteuil et al., 2002; Ito et al., 2003; Maia, 2019). For example, the distance between the Hollister transform and the nearest Louisville hotspot is approximately 400 km. The depth of the small age-offset (3.4 Myr) Hollister transform at the Pacific-Antarctic Ridge is only 2.99 km, which is significantly shallow among the compiled OTFs (Figure S7 in Supporting Information S1). The shallow valley nearly disappears around the ridge-transform intersections (Figure S8a in Supporting Information S1), which may be caused by the redistribution of plume flux from the nearby Louisville hotspot (Small, 1995). Figure S7 in Supporting Information S1 shows the effect of nearby hotspots. Some OTFs (e.g., Blanco D, Hollister, etc.) seem to be affected by nearby hotspots, as expressed in the shallow depth likely due to crustal thickening. However, we also observed some deep transforms (e.g., Ter Tholen, Bouvet, Shaka, etc.) that are close to hotspots, suggesting a relatively weak impact of nearby hotspots, which may correspond to low plume flux (e.g., Sibrant et al., 2019). Besides, there are also a number of shallow transforms (e.g., SEIR 96E W, Raitt W) without any nearby hotspot (within 1,000 km), indicating that the impact of a nearby hotspot is not systematic.

Further, changes in plate motion may affect the structure of transform faults. Previous observation suggested that OTFs do not precisely parallel plate motion (Mishra & Gordon, 2016). Therefore, small variations in spreading direction may cause an additional component of either compression or extension acting along an OTF, which, in turn, may affect either estimation of depth or width and thus contribute to the profound scatters observed in statistics. For example, in some cases, shallow transforms show indications for transpressive tectonics (Figures S8c–S8d in Supporting Information S1), which may result from intense deformation in response to the reorientation of the spreading center (Carbotte & Macdonald, 1994; Maia et al., 2016; Pockalny, 1997; Wolfson-Schwehr & Boettcher, 2019). Positive flower structures, for example, developed along the Chain transform (Figure 1b), result from transpression along the fault (Harmon et al., 2018) and thus may induce uplift of the seafloor along the axis of the transform valley leading to shallow overall depths. Furthermore, changes in plate motion can also create transtension across the transform (Bonatti et al., 2005; Tucholke & Schouten, 1988; Wolfson-Schwehr & Boettcher, 2019). Along the Kane transform, Pockalny et al. (1996) suggested that changes in plate motion caused transtension, contributing to the widening of the valley and formation of transverse ridges flanking the transform by flexural response. In addition, a recent study (Zhang et al., 2022) on OTFs at Pacific Antarctic Ridge indicated that, in response to plate rotation, off-transform normal faults and rift zones might even take place, adding to the complexity in the morphology of transform systems.

The key feature of most OTFs is a deep valley extending along the active strike-slip fault (Wolfson-Schwehr & Boettcher, 2019). Our statistical analysis shows the spreading rate and age-offset dependence of the morphological characteristics of OTFs. The correlation between transform morphology and spreading rate turns out to be weak, while a more robust relationship that transform valleys get deeper and wider with increasing age-offset, links the surface deformation to the cross-transform extension predicted by numerical models, as discussed above. The larger age-offset causes greater extension at OTFs (Furlong et al., 2001; Grevemeyer et al., 2021) and consequently wider and deeper valleys as revealed by our statistical approach.

5. Conclusions

Morphological variability of global oceanic transform faults derived from shipborne bathymetric data and its dependence on related tectonic parameters were systematically analyzed in this study. Our statistical results suggest that

1. OTFs from ultraslow- and slow-spreading ridges tend to have large-age-offset, long, wide, and deep valleys, while at intermediate-spreading ridges, transforms show mostly small age-offsets, where morphology demonstrates high complexities. However, correlations between morphological parameters and spreading rate are weak.
2. Age-offset is the key feature governing transform morphology rather than spreading rate, as age-offset scales better with morphological parameters. At a global scale, larger age-offsets correspond to longer, wider, and deeper valleys. Thus, it is indicated that, in addition to strike-slip motion, cross-transform extension is an important process acting on oceanic transform plate boundaries.

3. Scatters observed in the correlations between morphological characteristics and age-offset indicate that, in addition to the extension, there are also secondary processes affecting transform morphology, such as nearby hotspots and changes in plate motion.

Data Availability Statement

Bathymetric data compiled from open sources are available at http://doi.org/10.5281/zenodo.4774185.

Acknowledgments
The authors thank Kyoko Okino, Marcia Maia, Marco Ligi, and Nicholas Harmon, who kindly contributed additional bathymetric data to this research. Colin Devey, Yuhan Li, Ingo Klaucke, and Anouk Beniest provided helpful feedback during the completion of this work. This manuscript benefited greatly from constructive reviews by three anonymous referees. Yu Ren thanks funding from the China Scholarship Council (201904910466). Open access funding enabled and organized by Projekt DEAL.

References

Bonatti, E., Brunelli, D., Buck, W. R., Cipriani, A., Fabretti, P., Ferrante, V., et al. (2005). Flexural uplift of a lithospheric slab near the Vema transform (Central Atlantic): Timing and mechanisms. *Earth and Planetary Science Letters*, *240*, 642–655. https://doi.org/10.1016/j.epsl.2005.10.010

Brink, U. S., Coleman, D. F., & Dillon, W. P. (2002). The nature of the crust under Cayman Trough from gravity. *Marine and Petroleum Geology*, *19*(8), 971–987. https://doi.org/10.1016/S0264-8172(02)00132-0

Carbotte, S. M., & Macdonald, K. (1994). Comparison of seafloor tectonic fabric at intermediate, fast, and super fast spreading ridges: Influence of spreading rate, plate motions, and ridge segmentation on fault patterns. *Journal of Geophysical Research*, *99*(B7), 13609–13631. https://doi.org/10.1029/93JB02971

Cessaro, R. K., & Hussong, D. M. (1986). Transform seismicity at the intersection of the oceanographer fracture zone and the Mid-Atlantic Ridge. *Journal of Geophysical Research*, *91*(B5), 4839–4853. https://doi.org/10.1029/JB091iB05p04839

Collette, B. (1974). Thermal contraction joints in a spreading seafloor as origin of fracture zones. *Nature*, *251*, 299–300. https://doi.org/10.1038/251299a0

Dauteuil, O., Bourgeois, O., & Mauduit, T. (2002). Lithosphere strength controls oceanic transform zone structure: Insights from analogue models. *Geophysical Journal International*, *150*(3), 706–714. https://doi.org/10.1046/j.1365-246X.2002.01736.x

DeMets, C., Gordon, R. G., & Argus, D. F. (2010). Geologically current plate motions. *Geophysical Journal International*, *181*(1), 1–80. https://doi.org/10.1111/j.1365-246X.2009.04491.x

Escartín, J., & Cannat, M. (1999). Ultramafic exposures and the gravity signature of the lithosphere near the fifteen-twenty fracture zone (mid-Atlantic ridge, 14°–16.5°N). *Earth and Planetary Science Letters*, *171*(3), 411–424. https://doi.org/10.1016/S0012-821X(99)00169-7

Fornari, D. J., Gallo, D. G., Edwards, M. H., Madsen, J. A., Perfit, M. R., & Shor, A. N. (1989). Structure and topography of the Siqueiros transform fault system: Evidence for the development of intra-transform spreading centers. *Marine Geophysical Researches*, *11*(4), 263–299. https://doi.org/10.1007/BF00282579

Fox, P. J., & Gallo, D. G. (1984). A tectonic model for ridge transform ridge plate boundaries: Implications for the structure of oceanic lithosphere. *Tectonophysics*, *104*, 205–242. https://doi.org/10.1016/0040-1951(84)90124-0

Furlong, K. P., Sheaffer, S. D., & Malservisi, R. (2001). Thermal-rheological controls on deformation within oceanic transforms. *Geological Society, London, Special Publications*, *186*, 65–83. https://doi.org/10.1144/GSL.SP.2001.186.01.05

Gallo, D. G., Fox, P. J., & Macdonald, K. C. (1986). A Sea Beam investigation of the Clipperton transform fault: The morphotectonic expression of a fast-slipping transform boundary. *Journal of Geophysical Research*, *91*, 3455–3467. https://doi.org/10.1029/JB091iB03p03455

Gerya, T. V. (2010). Dynamical instability produces transform faults at mid-ocean ridges. *Science*, *329*, 1047–1050. https://doi.org/10.1126/science.1191349

Gerya, T. V. (2012). Origin and models of oceanic transform faults. *Tectonophysics*, *522–533*, 34–54. https://doi.org/10.1016/j.tecto.2011.07.006

Gerya, T. V. (2013). Three-dimensional thermomechanical modeling of oceanic spreading initiation and evolution. *Physics of the Earth and Planetary Interiors*, *214*, 35–52. https://doi.org/10.1016/j.pepi.2012.10.007

Grevemeyer, I., Rüpke, L. H., Morgan, J. P., Iyer, K., & Devey, C. W. (2021). Extensional tectonics and two-stage crustal accretion at oceanic transform faults. *Nature*, *591*, 402–407. https://doi.org/10.1038/s41586-021-03278-9

Harmon, N., Rychert, C., Agius, M., Tharimena, S., Le Bas, T., Kendall, J. M., & Constable, S. (2018). Marine geophysical investigation of the Chain fracture zone in the equatorial Atlantic from the PI-LAB experiment. *Journal of Geophysical Research: Solid Earth*, *123*(11), 11016–11030. https://doi.org/10.1029/2018JB015982

Ito, G. (2021). Oceanic fault zones reconstructed. *Nature*, *591*, 376–377. https://doi.org/10.1038/d41586-021-00639-2

Ito, G., Lin, J., & Graham, D. (2003). Observational and theoretical studies of the dynamics of mantle plume–mid-ocean ridge interaction. *Reviews of Geophysics*, *41*, 1017. https://doi.org/10.1029/2002RG000117

Ligi, M., Bonatti, E., Bortoluzzi, G., Carrara, G., Fabretti, P., Gilod, D., et al. (1999). Bouvet triple junction in the south Atlantic: Geology and evolution. *Journal of Geophysical Research: Solid Earth*, *104*(12), 29365–29385. https://doi.org/10.1029/1999JB900192

Ligi, M., Bonatti, E., Gasperini, L., & Poliakov, A. N. B. (2002). Oceanic broad multifault transform plate boundaries. *Geology*, *30*(1), 11–14. https://doi.org/10.1130/0091-7613(2002)030<0011:Obmtpb>2.0.Co;2

Luo, Y., Lin, J., Zhang, F., & Meng, W. (2021). Spreading rate dependence of morphological characteristics in global oceanic transform faults. *Acta Oceanologica Sinica*, *40*(5), 1–64. https://doi.org/10.1007/s13131-021-1722-5

Maia, M. (2019). Topographic and morphologic evidences of deformation at oceanic transform faults: Far-field and local-field stresses. In J. C. Duarte (Ed.), *Transform plate boundaries and fracture zones* (pp. 61–87). Elsevier. https://doi.org/10.1016/B978-0-12-812064-4.00003-7

Maia, M., Sichel, S., Briais, A., Brunelli, D., Ligi, M., Ferreira, N., et al. (2016). Extreme mantle uplift and exhumation along a transpressive transform fault. *Nature Geoscience*, *9*(8), 619–623. https://doi.org/10.1038/Ngeo2759

Mishra, J. K., & Gordon, R. G. (2016). The rigid-plate and shrinking-plate hypotheses: Implications for the azimuths of transform faults. *Tectonics*, *35*, 1827–1842. https://doi.org/10.1002/2015TC003968

Morgan, J. P., & Forsyth, D. W. (1988). Three-dimensional flow and temperature perturbations due to a transform offset: Effects on oceanic crustal and upper mantle structure. *Journal of Geophysical Research*, *93*(B4), 2955–2966. https://doi.org/10.1029/JB093iB04p02955

Okino, K., Nakamura, K., & Sato, H. (2015). Tectonic background of four hydrothermal fields along the Central Indian ridge. In J. Ishibashi, K. Okino & M. Sunamura (Eds.), *Subseafloor biosphere linked to hydrothermal systems* (pp. 133–146). Springer. https://doi.org/10.1007/978-4-431-54865-2_11

Pockalny, R. (1997). Evidence of transpression along the Clipperton transform: Implications for processes of plate boundary reorganization. *Earth and Planetary Science Letters*, *146*, 449–464. https://doi.org/10.1016/S0012-821X(96)00253-1

Pockalny, R., Gente, P., Buck, R. (1996). Oceanic transverse ridges: A flexural response to fracture-zone-normal extension. *Geology*, *24*(1), 712–n. https://doi.org/10.1130/0091-7613(1996)024<0071:otrafr>2.3.co;2

Pockalny, R. A., Detrick, R. S., & Fox, P. J. (1988). Morphology and tectonics of the Kane transform from sea beam bathymetry data. *Journal of Geophysical Research*, *93*(B4), 3179–3193. https://doi.org/10.1029/JB093iB04p03179

Ryan, W. B. F., Carbotte, S. M., Coplan, J. O., O'Hara, S., Melkonian, A., Arko, R., et al. (2009). Global multi-resolution topography synthesis. *Geochemistry, Geophysics, Geosystems*, *10*, Q03014. https://doi.org/10.1029/2008GC002332

Sandwell, D. T. (1986). Thermal stress and the spacings of transform faults. *Journal of Geophysical Research: Solid Earth*, *91*(B6), 6405–6417. https://doi.org/10.1029/JB091iB06p06405

Searle, R. C. (1986). GLORIA investigations of oceanic fracture zones: Comparative study of the transform fault zone. *Journal of the Geological Society*, *143*(5), 743–756. https://doi.org/10.1144/gsjgs.143.5.0743

Seton, M., Müller, R. D., Zahirovic, S., Williams, S., Wright, N. M., Cannon, J., et al. (2020). A global data set of present-day oceanic crustal age and seafloor spreading parameters. *Geochemistry, Geophysics, Geosystems*, *21*, e2020GC009214. https://doi.org/10.1029/2020GC009214

Sibrant, A. L. R., Maia, M., Mittelstaedt, E., & Graham, D. W. (2019). Variable crustal production originating from mantle source heterogeneity beneath the South East Indian Ridge and Amsterdam-St. Paul Plateau. *Geochemistry, Geophysics, Geosystems*, *20*, 4635–4653. https://doi.org/10.1029/2019GC008419

Small, C. (1995). Observations of ridge-hotspot interactions in the Southern Ocean. *Journal of Geophysical Research*, *100*(B9), 17931–17946. https://doi.org/10.1029/95JB01377

Sykes, L. R. (1967). Mechanism of earthquakes and nature of faulting on the mid-oceanic ridges. *Journal of Geophysical Research*, *72*(8), 2131–2153. https://doi.org/10.1029/JZ072i008p02131

Tozer, B., Sandwell, D. T., Smith, W. H. F., Olson, C., Beale, J. R., & Wessel, P. (2019). Global bathymetry and topography at 15 arc sec: SRTM15+. *Earth and Space Science*, *6*, 1847–1864. https://doi.org/10.1029/2019EA000658

Tucholke, B., & Schouten, H. (1988). Kane fracture zone. *Marine Geophysical Researches*, *10*, 1–39. https://doi.org/10.1007/BF02424659

Turcotte, D. L. (1974). Are transform faults thermal contraction cracks? *Journal of Geophysical Research*, *79*(17), 2573–2577. https://doi.org/10.1029/JB079i017p02573

Whitmarsh, R. B., & Calvert, A. J. (1986). Crustal structure of Atlantic fracture zones — I. The Charlie-Gibbs fracture zone. *Geophysical Journal International*, *85*(1), 107–138. https://doi.org/10.1111/j.1365-246X.1986.tb05174.x

Wilcock, W. S. D., Purdy, G. M., & Solomon, S. C. (1990). Microearthquake evidence for extension across the Kane transform fault. *Journal of Geophysical Research*, *95*(B10), 15439–15462. https://doi.org/10.1029/JB095iB10p15439

Wilson, J. T. (1965). A new class of faults and their bearing on continental drift. *Nature*, *207*, 343–347. https://doi.org/10.1038/207343a0

Wolfson-Schwehr, M., & Boettcher, M. S. (2019). Global characteristics of oceanic transform fault structure and seismicity. In J. C. Duarte (Ed.), *Transform plate boundaries and fracture zones* (pp. 21–59). Elsevier. https://doi.org/10.1016/B978-0-12-812064-4.00002-5

Yu, Z., Singh, S. C., Gregory, E. P. M., Maia, M., Wang, Z., & Brunelli, D. (2021). Semi-brittle seismic deformation in high-temperature mantle mylonite shear zone along the Romanche transform fault. *Science Advances*, *7*(15), eabf3388. https://doi.org/10.1126/sciadv.abf3388

Zhang, F., Lin, J., Zhou, Z., Yang, H., & Morgan, J. P. (2022). Mechanism of progressive broad deformation from oceanic transform valley to off-transform faulting and rifting. *Innovation*, *3*(1), 100193. https://doi.org/10.1016/j.xinn.2021.100193

References From the Supporting Information

Morgan, W. J., & Morgan, J. P. (2007). Plate velocities in the hotspot reference frame. In G. R. Foulger & D. M. Jurdy (Eds.), *Plates, plumes and planetary processes: Geological society of America special paper 430* (pp. 65–78). The Geological Society of America. https://doi.org/10.1130/2007.2430(04)

Tebbens, S. F., Cande, S. C., Kovacs, L., Parra, J. C., LaBrecque, J. L., & Vergara, H. (1997). The Chile ridge: A tectonic framework. *Journal of Geophysical Research*, *102*(B6), 12035–12059. https://doi.org/10.1029/96JB02581